THUMSv7 Response and Injury Assessment Using Parametrised Restraints in a Stock Car Racing Environment

Timothy Edinger[1], Michal Suchozebrski[1], Neal Morgan[1], John Patalak[2], Sayak Muhkerjee[2], Bronislaw Gepner[1]

Abstract Motorsports crashes occur with greater frequency and severity than passenger vehicle crashes, yet injury rates among professional drivers remain comparatively low due to highly optimised restraint systems. This study investigates the sensitivity of restraint system parameters on thoracic and lumbar injury risk prediction in a stock car racing environment using the THUMS AM50 v7 Human Body Model (HBM). A detailed NASCAR stock car environment was modeled in LS-DYNA, incorporating a fully parametrised restraint system. Fifty-four frontal crash simulations were conducted across four parametric sub-studies. Thoracic and lumbar injury outcomes were assessed using HBM-specific injury risk functions for rib fractures and lumbar vertebral fractures. Multivariate stepwise regression models were developed to quantify the influence of restraint parameters on predicted injury risk. Results indicate that seat foam stiffness, shoulder and anti-submarine belt anchorage, belt configuration, belt tension, and FHR type significantly affect injury risk, with differing trends observed between thoracic and lumbar regions. This work provides HBM response insights for a NASCAR environment including restraint design influences relevant to thoracolumbar injury mitigation in motorsports as well as the performance of the THUMS AM50 v7 in a non-standard restraint environment.

Keywords Human Body Models, Lumbar Spine Injury, Motorsports, Parametric Study, Thoracic Injury

I. INTRODUCTION

While motorsports places safety as a primary priority, it also emphasises speed, competition, and high-performance driving, resulting in a greater likelihood of crashes and on-track incidents, whereas passenger vehicle operation occurs on public roadways, regulated settings designed to minimise risk. A study performed by the National Association for Stock Car Auto Racing (NASCAR) found that NASCAR race cars were 134 times more likely to experience a crash than passenger vehicles per mile driven [6]. Despite the increased occurrence of crashes in motorsports, the rate of injuries per crash is 9.3 times lower for a NASCAR driver than a passenger vehicle occupant [6]. One of the major reasons for the gulf in injury incidence is the robust safety systems employed by NASCAR. As opposed to passenger vehicle restraint systems, which must be designed with comfort and convenience in mind to encourage usage [11], motorsports restraints can be more extensive, with compulsory usage and adjustment. NASCAR driver restraints include an expanded seat belt system consisting of seat belts with seven or nine anchor locations, more robust and protective seats, frontal head restraint (FHR) devices, and helmets, greatly reducing injury exposure despite common and severe impacts [7].

Anthropomorphic Test Devices (ATDs) have long been used in both passenger vehicle and motorsports safety research as surrogates for restraint development [12–13]. While ATD's are an indispensable tool, they also are limited by their design and included instrumentations in specific loading conditions. ATDs are typically designed for one direction of applied pulse and may only be biofidelic for a single or narrow range of postures [14]. Furthermore, ATDs may lack instrumentation and biofidelity in some body regions, such as the lumbar spine, limiting their ability to fully investigate injury mechanisms in these areas. As a result, these limitations constrain the applicability and overall effectiveness of ATDs in some specific injury mechanism investigations or environments.

The emergence of human body models (HBMs) provides an opportunity for injury prediction and analysis in unique environments with varied restraint parameters without as large of a time and monetary cost as for traditional sled and dummy testing. Recently developed injury risk functions (IRFs) for the thorax and lumbar spine also provide improved injury prediction for these body regions, designed for use with HBMs. While all occupant protection tools have limitations, HBMs are closer representations of the human body and are intended

[1] University of Virginia Center for Applied Biomechanics, Charlottesville, Virginia, U.S.A.

[2] National Association for Stock Car Auto Racing, LLC, Daytona Beach, FL, U.S.A.

to be applicable to omni-directional loading and varied postures. HBMs are also not limited by physical design factors for instrumentation, so they have a wider range of data that can be collected and thus injuries that can be predicted. Because HBM instrumentation is not limited by physical constraints, HBMs have additional applicability to new injury reference data and injury risk functions, as the required instrumentation can generally be added after surrogate development.

These factors provide a unique opportunity to study the effects of varied restraint parameters on the injury predicted with the HBMs, as well as to investigate the validity of HBMs and IRFs in a non-passenger vehicle restraint environment. A review of available vehicle crash and injury databases reveals that the thorax is one of the most frequently injured regions in motor vehicle collisions (MVCs) [1–3]. Lumbar injuries are also prevalent in MVCs, specifically in frontal collisions [4-5]. A study performed by NASCAR also found that thoracic and lumbar injuries constituted a larger portion of AIS2+ injuries across motorsports crashes from 2011–2018, though thoracic injuries have not been observed in recent years [6]. Two recently developed IRFs, for thoracic and lumbar fracture risks have been tuned for HBM usage and provide an opportunity for more accurate injury risk prediction in a simulation environment. The Forman *et al.* thoracic IRF directly correlates post mortem human subject (PMHS) data to HBM injury prediction through the tuning of a strain-based IRF [8] and the Tushak lumbar IRF correlates moment, force and matched lumbar flexion angle from PMHS data to HBM specific risk functions [9], both of which contribute to overall increased accuracy of injury prediction.

The goal of this study was to investigate the sensitivity of driver restraint parameters on the potential for driver injury using the THUMS AM50 v7 human body model. The parameters examined included seat belt material, seat belt type, seat belt pre-tensioning, anchorage location, frontal head restraint (FHR) type and configuration, seat material, and driver mass. Injury assessment focused on the thorax and lumbar spine, as these regions accounted for a substantial proportion of AIS-2+ injuries observed in motorsports crashes. Multi-variate regression models were applied to characterise the effects of the varied restraint parameters on predicted thoracic and lumbar injury outcomes.

I. METHODS

Simulation Environment and Parameters

Full-body simulations were performed using the THUMS v7.1 50^{th} male (AM50) with normal muscle activation as distributed with the THUMS model in a NASCAR provided stock car racing environment using LS-DYNA version 14.0.0, mpp971, openmpi. The THUMS v7.1 AM50 was validated across multiple body regions through comparison to PMHS tests [22], with improvements in the responses of the abdomen, lumbar spine, and internal organs among other parts. The simulation environment was modelled after the interior of a NASCAR stock car, seen in Fig. 1. This environment was validated using ATD's and HBM's in sled tests, as well as through specific material testing of seat components [25–26]. The stock car environment was modified to allow parametrisation of the restraint system as necessary. Settling pre-simulations were performed to reduce overall simulation time and ensure proper belt engagement across varied arrangements. Four such pre-simulations were created, one for each seat foam and FHR combination. The pre-simulations were conducted from the same initial posture and position, with gravity applied and constraints fixing the hands to the steering wheel and feet to the foot-rest. A simplified NASCAR crash pulse was applied to this stock car environment, with a peak acceleration of 34g's. Additional information on the applied pulse can be found in appendix C.

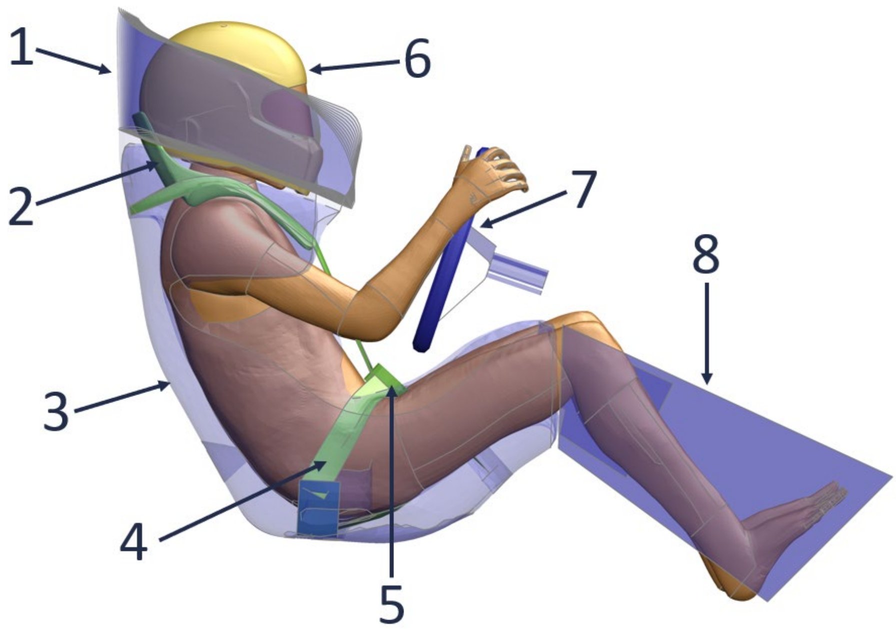

Fig. 1. THUMS AM50 v7 Positioned in a NASCAR stock car racing environment with labelled restraints. 1: Head surround and foam, 2: HANS FHR, 3: Seat shell and SFI Foundation 45.2 foam, 4: Seat belt, 5: Camlock, 6: Helmet, 7: Steering wheel, 8: Footrest and knee bolster.

Multiple parametric studies were performed including 11 variables, as seen in Table 1. Six parameters related to the seat belt restraints were varied, including the anchor locations of the shoulder, lap, and anti-submarine belts, the belt material type, and the belt configuration (7pt or 9pt belt). The shoulder, lap, and anti-submarine belt anchor locations were varied over three levels to adjust the belt path from 0 to -30 degrees for the shoulder belt, -20 to -45 degrees for the lap belt, and 0 to -70 degrees for the anti-submarine belt. Belt routing was performed using the OASYS Primer (Oasys Ltd., Solihull, United Kingdom) belt routing tool to ensure consistent belt fit across the different settled positions. Visualisation of the seat belt anchor levels can be found in appendix A1-3.

Table 1. Parameter list detailing units, levels of variation, minimum, maximum, default value, and parameter types.

Parameter	Units	Levels	Min	Max	Default	Type
FHR Tether Length	mm	3	0	20	0	Numerical
FHR Type	-	2	HANS	Hybrid	HANS	Categorical
Seat Belt Anchors	-	2	7pt	9pt	7pt	Categorical
Shoulder Belt Anchor Angle XZ	deg.	3	0	-30	-15	Numerical
Lap Belt Anchor Angle XZ	deg.	3	-20	-45	-35	Numerical
Anti-Submarine Belt Angle XZ	deg.	3	0	-70	-35	Numerical
Belt Material Curves (Fabric)	Stress/Strain	2	Polyester	UHDPE	Polyester	Categorical
Seat Belt Pre-Tension	N	5	-100 (Slack)	150 (Tension)	100	Numerical
Seat Foam Material	Stress/Strain	2	SFI 45.2	NASCAR Opt. 2	SFI 45.2	Categorical
Head Foam Material	Stress/Strain	2	SFI 45.2	NASCAR Opt. 2	NASCAR Opt. 2	Categorical
Occupant Mass	kg	3	68	90	77	Numerical

The seat belt configuration also was varied for use with the HANS FHR, though not with the Hybrid FHR due to its design constraints. A typical 7pt belt used in NASCAR consists of a camlock release mechanism attached to two shoulder, two lap, two anti-submarine, and one negative g belt which then connect to their respective anchor locations on the seat. A 9pt belt differs only in the shoulder belts, characterised by shoulder belts which split into two unique belts near the bottom of the HANS collar, both of which anchor to the seat behind the driver, resulting in four shoulder belt anchorages. Typically, the under-shoulder belt is three inches wide and passes under the FHR, while the over belt passes over the FHR and is two inches wide. The 9pt belt typically has about a 75mm gap between the bottom tips of the HANS FHR and the merge point of the two shoulder belts. The anchorage of these two shoulder belts was aligned on their inner edges, closest to the centreline of the driver. A diagram of the 9pt belt can be seen in appendix A4-5.

Seat belt material types were also varied using models of Polyester and ultra-high-density polyethylene (UHDPE) belts, with physical testing data. The polyester belt is characterised by a mostly linear loading regime, while the UHDPE belt is more compliant than the polyester belt until a strain of approximately 0.09 where it becomes and remains stiffer. The belt loading curves can be found in appendix B.

The last parameter relating to belt restraints is the belt tension. In this study, the LS-DYNA *AIRBAG_REFERENCE_GEOMETRY (ARG) card was used to apply equivalent belt tension to all belt sections. The ARG card uses reference geometry, in this case a scaled version of each seat belt section, as an adaptation target reference for the seat belt section. A longer reference geometry will cause the belt section to expand, creating slack in the belt section, and a shorter reference belt will cause the belt section to contract, creating tension in the belt section. Calibration simulations were completed to determine the appropriate reference length scale factors for ARG tension. Each belt was modelled using two sections, one *MAT_034_FABRIC layer with elform 9, and a second *MAT_001_ELASTIC layer with elform 2. The fabric layer constitutes the primary response and is the material modelled after polyester and UHDPE, while the elastic layer increases the numerical stability when ARG is applied.

Three parameters related to the FHR were varied, FHR type, FHR to helmet tether length, and seat belt configuration. A model for the Hybrid FHR was developed from a CAD version of the 2014 Hybrid Pro Lightweight collar. The CAD model for the collar was meshed and geometry imported into LS-DYNA, where belt routing for the harness was performed, again using the OASYS Primer (Oasys Ltd., Solihull, United Kingdom) belt routing tool. Additional information is found in appendix A6. The added tether length parameter is only used for the Hybrid FHR because prior research has shown variation of HANS FHR tether length to have a minimal effect on ATD response [20].

The last parameters varied pertain to the foam materials and occupant mass. The NASCAR stock car model used two foams, SFI 45.2 [17] and NASCAR Option2 for the seat and head foams respectively. The foam materials were provided by NASCAR and were modelled as *MAT_057_LOW_DENSITY_FOAM. The SFI 45.2 is a stiffer foam [18], and NASCAR Option2 is a softer foam [19]. Occupant mass was varied by scaling the mass of the THUMS HBM from a base of 77kg to 68 or 90kg using the *INCLUDE_TRANSFORM card. 68 and 90kg were chosen as representative of the weight bounds of NASCAR driver population. This method of mass scaling changes the density of the HBM instead of changing the size, which may not fully represent real occupant mass variation.

Simulation Matrix and Instrumentation

To reduce the overall number of simulations, a full factorial study of these parameters was not performed. Instead, the parameters were divided into 'sub-studies' of variables thought to be related to or interact with each other. Four sub-studies were conducted, investigating the following parameters: (1) A seat study varying seat/head foam material and HBM mass, (2) A seat belt study varying seat belt material and seat belt pre-tension/slack, (3) A seat belt anchor study varying shoulder, lap, and anti-submarine belt anchor locations, and (4) And a FHR study varying 7/9-point belt, shoulder belt anchor location, FHR type and tether length, for a total of 54 simulations. A multi-variate stepwise least-squares regression model was created for each combination of sub-study and injury metric for a total of eight regressions.

The Human Injury Prediction Suite (HIPS) was used for instrumentation of the model and collection of the data relevant to these IRFs. HIPS provides full-body instrumentation and injury predictions, and injury visualisation for the THUMS AM50 v7 HBM and was used for the LS DYNA instrumentation of THUMS and simulation post-processing of this study [10]. An age of 39 was used as an IRF covariate when applicable.

II. RESULTS

Of the fifty-four simulations were conducted for this study with and average runtime of 23 hours and one error termination encountered prior to maximum excursion (Defined by maximum excursion of the sternum). The simulation with early-termination was removed from the study. The remaining 53 simulations were used as inputs for a statistical analysis. From the simulation results, strains from each rib element and section forces and moments from the lumbar vertebrae collected for injury prediction of rib and lumbar fracture.

There were two foci for injury outcomes, thoracic and lumbar fracture, as these have established IRFs for the

THUMS HBM and constitute a recent area of injury mechanism focus by NASCAR. For thoracic injury the Forman strain-based IRF tuned to the THUMS AM50 v7 was used, involving the use of a local strain based IRF for each rib, which is then used as the input in a probabilistic model that predicts the likelihood of an overall number of ribs fractured in a specific scenario, in this case three plus (3+) ribs fractured [8]. The specific formulation of this IRF has been updated from the 2022 paper to include combined frontal and side impact injury data, as well as to use MPS95 strain values instead of MPS100. Results of two lumbar IRFs are displayed in Table 2, a PMHS tuned function and a THUMS equal flexion tuned function.

Lumbar injury was predicted using the Tushak PMHS lumbar fracture IRF, which uses a ratio of force, moment, and cross-sectional area of the lumbar vertebrae to predict the fracture risk [9]. However, Gepner *et al*., 2022 [24] found a significant difference in response of the lumbar spine of HBMs as compared to PMHS. Consequently, a formulation of the lumbar IRF has since been updated for use with the THUMS HBM, tuning the function to account for moment–angle response discrepancy between THUMS and PMHS [15]. The new updated THUMS specific lumbar IRF, considers moment-angle differences and proposes a formulation that assumes fracture occurrence at a matched flexion angle between THUMS and PMHS. To evaluate both approaches, both the PMHS based and THUMS based IRFs were used in this study. Since both functions produced a consistent regression response, only PMHS tuned function was used for the regression analysis, and the THUMS function was monitored to evaluate change in overall risk.

The independent variables for each regression were the parameters varied in its respective sub-study, as well as the first-degree interactions of the parameters. The dependent variables were the predicted risks of three plus ribs fractured or the risk of lumbar vertebrae L1 fracture. Three plus ribs fractured was selected as the predictor for thoracic injury due to it giving a representation of overall thoracic injury as opposed to specific ribs injured, with a broad range of predicted injury risks, ranging from 17.5-95.4%. The first lumbar vertebra received the highest injury risk prediction and had the widest range of predictions across all simulations from 15.2-61.9%, using the PMHS based IRF, and was used as the representative lumbar injury response. Stepwise selection of regression terms was performed to determine parameter coefficients of significance at a 95% confidence level for each sub-study, with entry and exit thresholds of p<=0.05 and 0.1 respectively. The significant parameter coefficients and a constant were then used to create a regression utilising the Stats Models python library ordinary least squares regression function [16]. The selected input parameters for these regressions can be found in Fig. 2-3 and the outputs of these regressions can be seen in Table 2 for each predicted injury metric. A comparison of the lumbar fracture IRFs can be found in appendix D.

Table 2. Results from the linear regressions performed for each sub-study and injury metric combination. Includes the range of predicted injury for each simulations subset and the adjusted R squared for each regression.

Sub-Study	Simulation Count	Predicted Injury Metric	Injury Range	Adjusted R Squared
1 (Seat)	12	3+ Ribs Fractured	47.1-76.1%	0.923
2 (Seat Belt)	10	3+ Ribs Fractured	34.1-93.1%	0.888
3 (Belt Anchor)	27	3+ Ribs Fractured	26.0-95.4%	0.934
4 (FHR)	15	3+ Ribs Fractured	17.5-94.2%	0.932
1 (Seat)	12	LV 1 Fracture (PMHS IRF)	18.3-61.9%	0.999
2 (Seat Belt)	10	LV 1 Fracture (PMHS IRF)	25.0-33.5%	0.861
3 (Belt Anchor)	27	LV 1 Fracture (PMHS IRF)	16.1-46.1%	0.953
4 (FHR)	15	LV 1 Fracture (PMHS IRF)	15.2-37.16%	0.987
1 (Seat)	12	LV 1 Fracture (THUMS IRF)	52.3-97.5%	0.991
2 (Seat Belt)	10	LV 1 Fracture (THUMS IRF)	68.4-77.5%	0.596
3 (Belt Anchor)	27	LV 1 Fracture (THUMS IRF)	44.8-95.08%	0.977
4 (FHR)	15	LV 1 Fracture (THUMS IRF)	39.6-85.3%	0.991

Before input into the regression, all variables are encoded according to the following rules: categorical parameters have the default, HANS for FHR type, set to zero and alternative value, Hybrid FHR type, set to one. The belt and seat material parameters are coded such that the softer materials have a value of zero and the stiffer have a value of one (SFI 45.2, UHDPE are stiff and NASCAR Option 2, Polyester are soft). Numerical parameters are scaled using z-score normalisation [16]. The parameter coefficients resulting from the regressions created are found in Fig. 2 for thoracic injury, and Fig. 3 for lumbar injury.

Thoracic Injury Results

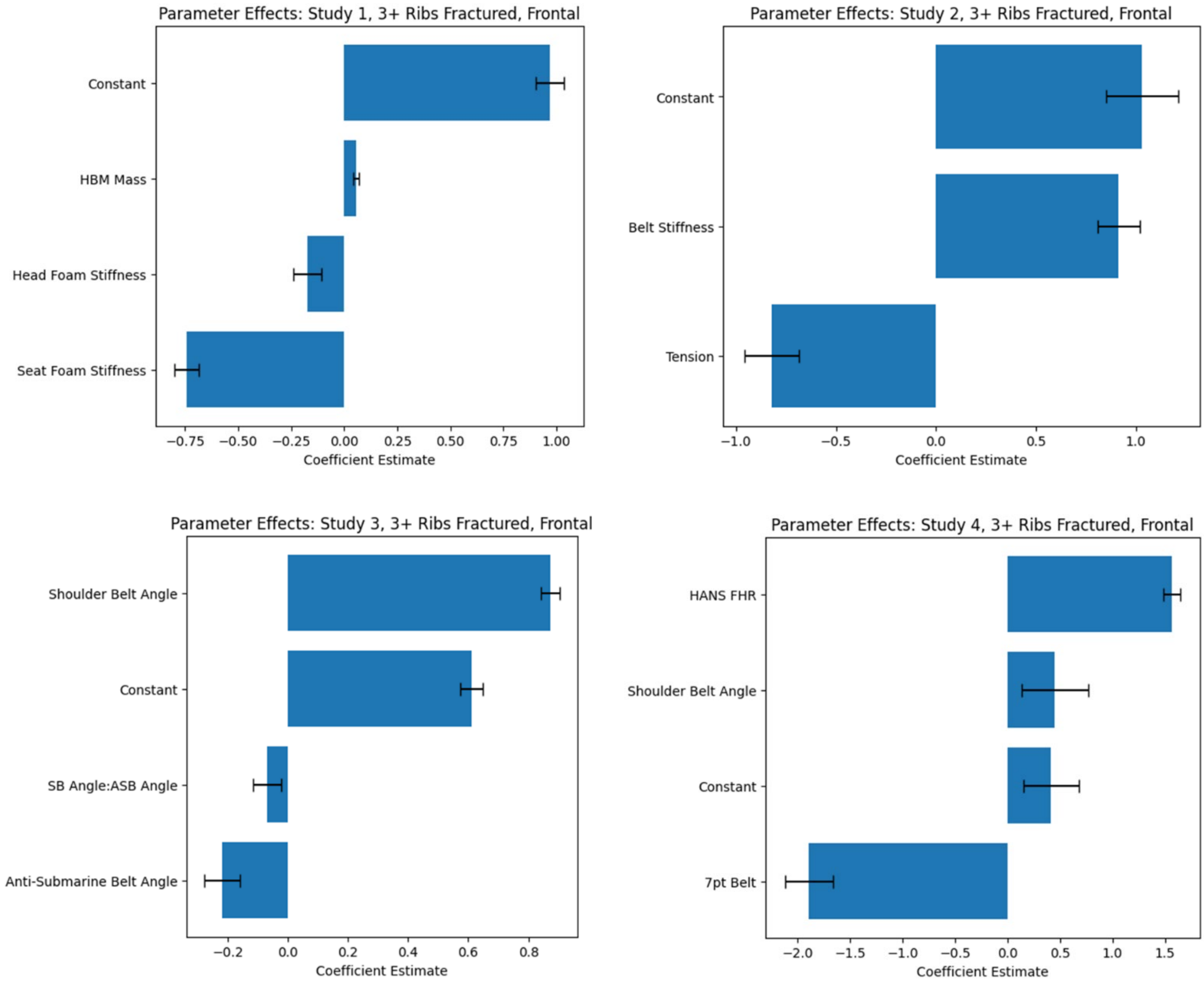

Fig. 2. Regression results and significant variables for the thoracic injury metric, studies 1-4. Interaction terms denoted with a ':'.

The parameter coefficients above represent the relative change in the regression for a given value of each parameter. The constant parameter signifies the value of injury risk with all parameters at their default, or average, values. Any non-zero parameter effect value signifies a move away from the average, and the sign signals the directionality of that change. A decrease in value correlates to a reduction in the predicted injury risk. For numerical variables, a positive coefficient signifies that a greater value increases predicted injury, while a negative coefficient again signifies the opposite.

The regression results for the first sub-study, parameters consisting of HBM mass, head foam stiffness, and seat foam stiffness found all parameters to be significant. Seat foam had the largest coefficient among these parameters, predicting that a stiffer seat foam reduces the predicted thoracic injury risk. The same conclusion was made for head foam, though to a lesser effect. Increasing HBM mass was also found to increase the predicted injury risk, though to a smaller degree than the foam stiffness parameters.

The second study involved belt stiffness (belt material) and belt tension parameters, both of which were found to be significant. Belt stiffness and belt tension were found to be roughly as significant as each other, with the stiffer belt material increasing predicted injury, and a higher belt tension reducing predicted thoracic injury.

The third study consisted of the seat belt anchor locations, for which the shoulder and anti-submarine belt anchors were found to be significant, though the lap belt was not. The regression shows that a lower shoulder belt anchor angle increases predicted thoracic injury and a more rearward anti-submarine belt anchor angle decreases predicted thoracic injury. A significant interaction term was also predicted between the shoulder belt and anti-submarine belt, which signifies that a rearward anti-submarine belt and more horizontal shoulder belt decreases predicted thoracic injury.

The fourth study consisted of the FHR, shoulder belt angle, FHR tether length, and seat belt configuration, finding that all parameters except for FHR tether length had a significant effect on predicted thoracic injury. The regression shows that FHR type and seat belt configuration had the largest effects on predicted thoracic injury, with the HANS FHR reducing injury as compared to the Hybrid FHR and the 9pt belt reducing injury as compared to the 7pt belt. Shoulder belt angle was found to have the same effect as in study 3.

Lumbar Injury Results:

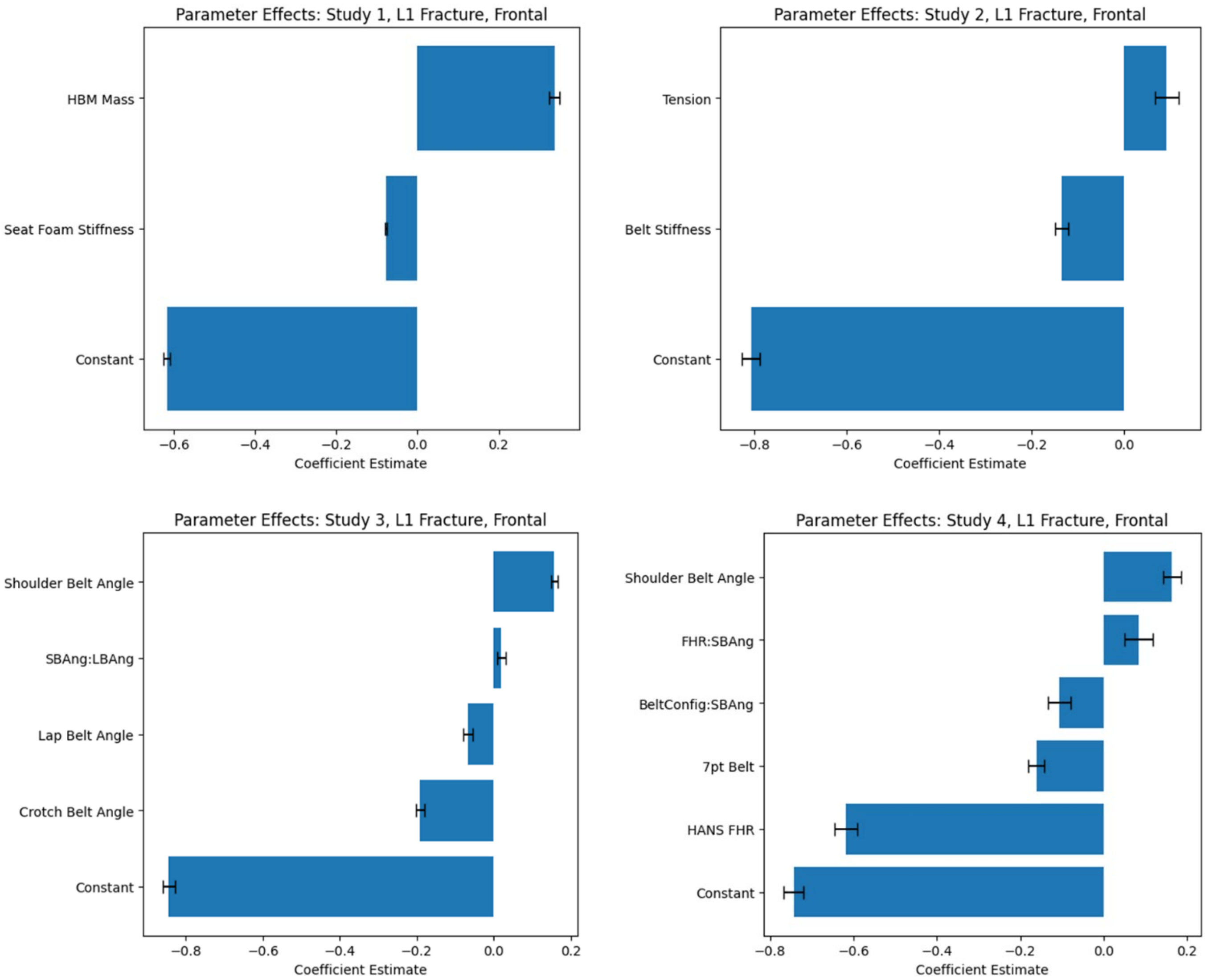

Fig. 3. Regression results and significant variables for lumbar injury metric, studies 1–4.

The regression for the first study predicts that HBM mass and seat foam are the significant variables, with head foam not being selected as significant. The regression shows that increased HBM mass and softer seat foam both increase predicted lumbar injury.

The second study selected belt tension and belt material as significant parameters, though with small coefficient estimates. This regression predicts that lower belt tension and a stiffer belt reduce predicted lumbar injury.

The third study selected all parameters as significant, as well as an interaction term between the shoulder and lap belt anchor angles. Regression predicts that a more horizontal shoulder belt angle reduces predicted lumbar injury, and that more rearward lap and anti-submarine belt anchor angles reduces predicted injury.

The fourth study selected shoulder belt angle, belt configuration, FHR type, and two interaction terms between the shoulder belt and belt configuration, and shoulder belt angle and FHR as significant parameters. The regression predicts that the Hybrid FHR and 9pt belt are more protective for lumbar injury than the HANS FHR and 7pt belt. The prediction for the shoulder belt angle effect is the same as for study 3. The interaction terms suggest that the combination of a Hybrid FHR and a less horizontal shoulder-belt anchor increases predicted lumbar injury, and that the combination of the 9pt belt and a less horizontal shoulder-belt anchor decreases predicted injury.

III. DISCUSSION

To physically interpret the parameter effect results it is helpful to compare results from specific simulations for which these parameters differ to understand the effects the parameter variation has on kinematic response and HBM performance. Parameter effect charts may give insight into how a variable changes a given injury response, but without understanding the underlying mechanics of the change in response, it is difficult to use that information to correctly inform restraint design and overall safety optimisation. Finding different parameters that act in similar ways to reduce injury helps to guide meaningful conclusions to make an occupant safer overall as opposed to a single specific condition. This analysis also aids in understanding whether the effects dictated by a given regression are practically significant or instead primarily a result of numerical noise or simulation instability. Strain contour comparisons for the thoracic injury case comparisons can be found in appendix E.

Thoracic Injury Prediction

The regressions developed for thoracic injury generally have clear relationships between parameter effects and kinematic response, except in the first sub-study. Study 1 selects all parameters of seat foam stiffness, head foam stiffness, and HBM mass to have a significant impact on predicted injury. Different settled positions were generated for each combination of seat foam and FHR, though these positions vary by at most 2mm, so difference in response due to changing seat foam was found to not be due to a difference in initial positioning. The difference in kinematics is more noticeable between the two seat foams, as can be seen through the greater excursion experienced by the softer seat foam simulation case, using softer seat foam in Fig. 4. No noticeable kinematic differences were found between simulations that varied only head foam, so the source of this parameter effect is unclear and may be due to simulation noise or effects that don’t directly pertain to HBM restraint. Head surround foam typically applies restraint forces in lateral and rear impacts, thus its lack of influence on HBM kinematics was expected. Higher HBM mass increases the excursion experienced, though the overall kinematic response remains similar, and the effect on predicted injury is small.

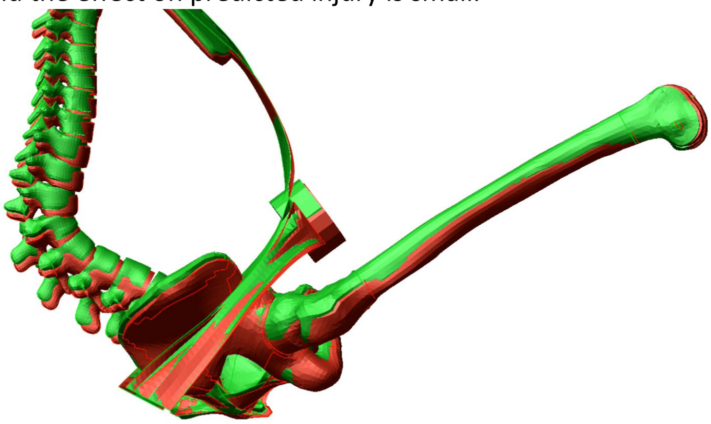

Fig. 4. Study 1 Kinematic Response Difference, Maximimum Excursion. Green: Stiffer Seat Foam (SFI 45.2), Red: Softer Seat Foam (NASCAR Option 2)

In the second sub-study, the HBM thorax response was effected by both seat belt tension and material. The earlier engagement from the seat belt was protective. This was achieved either through belt pretension (e.g. 150N belt tension) or by using the ployester belt materail which is characterised by higher tension at low strain (Appendix B). This difference can be seen in Fig. 5 and 6, which compare kinematics at maximum excursion for varied belt tension and material respectively. In both cases, the parameters that achieve the aforementioned effect (150N belt tension and polyester belt material) were more protecitve than alternative parameters. The case with the lowest predicted injury, involved a polyester belt and belt tension of 150N, while the case with the highest predicted injury used a UHDPE belt and -100N belt tension. The effect of belt pretension on kinematics is clear; a higher belt pretension restrains the HBM earlier and allows for less HBM inertia to be accumulated before maximum seat belt loading, while slack in the seat belt does the opposite. The seat belt material has a similar effect due to the difference in response of the belts. The polyester belt material linearly increases in stiffness for the majority of loading, while the UHDPE belt material begins relatively soft, and only becomes stiffer at a strain of roughly 0.09 where it rapidly increases in stiffness. This creates an effect, similar to varied belt tension, where the polyester belt material, loading consistently from the beginning of pulse application, is more protective for the HBM, reducing overall excursion and peak thoracic forces.

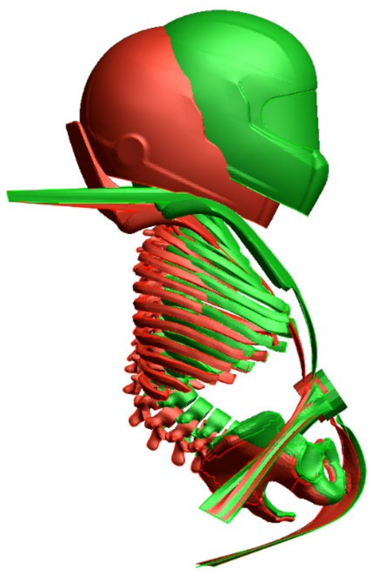

Fig. 5. Study 2 Kinematic Response Difference, Maximum Excursion. Green: -100N Belt Tension, Red: 150N Belt Tension

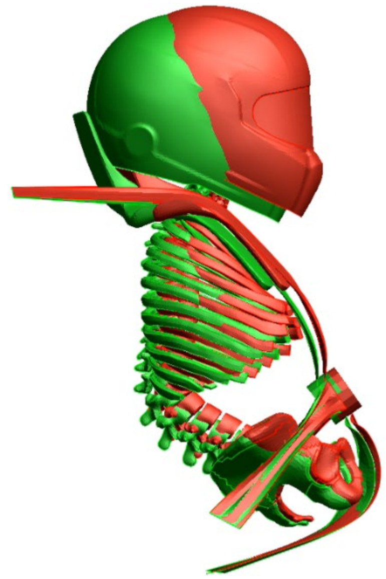

Fig. 6. Study 2 Kinematic Response Difference, Maximum Excursion. Green: Polyester Belt, Red: UHDPE Belt

The third sub-study, varying seat belt anchor locations, found the shoulder belt and anti-submarine belt anchor angles to be significant parameters. Kinematics of these differences can be found in Fig. 7 and 8 for the shoulder and anti-submarine belts respectively. The difference in shoulder belt angle influences both the torso kinematics of the HBM and the interaction of the FHR and HBM. The image in Fig. 7 showcases the difference in response from varied shoulder belt anchor angles, in which the zero-degree case experiences less torso compression and a larger angle between the seat belt and top of the HANS collar. This reduces the overall load on the torso as well as the forces at the interaction points of the HANS collar and HBM around R1 and R8. The change in anti-submarine belt angle has a different overall effect, slightly changing the forwards excursion of the HBM. The belt with the further rearward anchor location (Red HBM in Fig. 8) essentially acts as a spring due to its increased length, loading more gradually and reducing peak seat belt forces via increased belt elongation. The rearward anchor location also increases the wrap of the anti-submarine belts around the HBM. Race cars offer limited space for this rearward anchor location, thus the maximum effect of the longer anti-submarine belt is not fully achievable in the field.

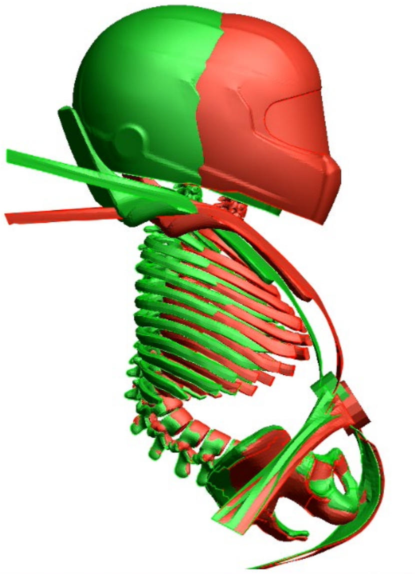

Fig. 7. Study 3 Kinematic Response Difference, Maximum Excursion. Green: 0-degree anchor, Red: 30-degree anchor.

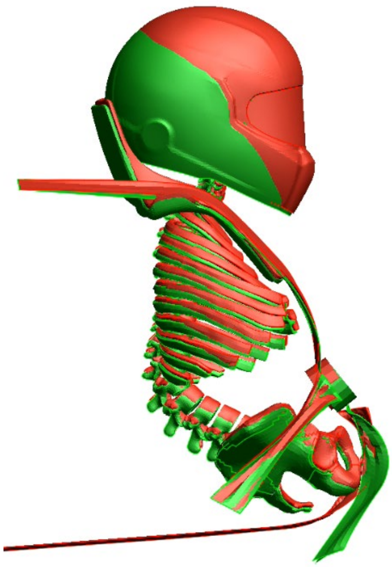

Fig. 8. Study 3 Kinematic Response Difference, Maximum Excursion. Green: 0-degree anchor, Red: 70-degree anchor.

The fourth sub-study for torso injury involved variations of the FHR and FHR related parameters, with the seat belt configuration and FHR type selected as significant. Fig. 9 and 10 show the differences between kinematic response and predicted injury for the HANS and Hybrid FHRs. In Fig. 9, a large difference in overall kinematics can be seen, with the Hybrid FHR case, in red, experiencing greatly increased head excursion and less forward translation of the torso as compared to the HANS FHR case. The images in Fig. 10 depict the predicted injury risks for the HANS and Hybrid FHRs. The left image, using the HANS FHR, shows a reduced spread of predicted rib fractures, with a force concentration around R1/R8, while the Hybrid FHR experiences a force concentration around R1, then a spread of increased loading from R2-R10. This difference may be exacerbated, as the HANS collar typically is used with a padded layer underneath which would spread out the loading across more of the thorax, likely reducing predicted injury, though the padding was not modelled for this study. Even without the additional padding, the HANS FHR reduces overall predicted injury due to a more favorable spread of thoracic loads.

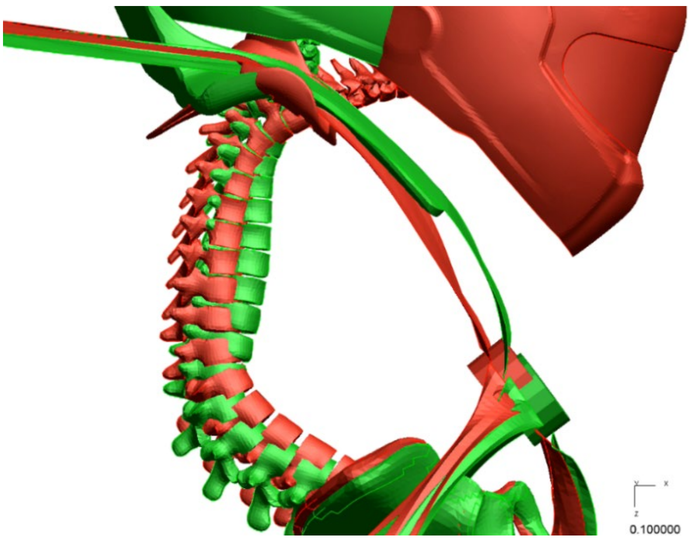

Fig. 9. Study 4 Kinematic Response Difference, Maximum Excursion. Green: HANS FHR, Red: Hybrid FHR.

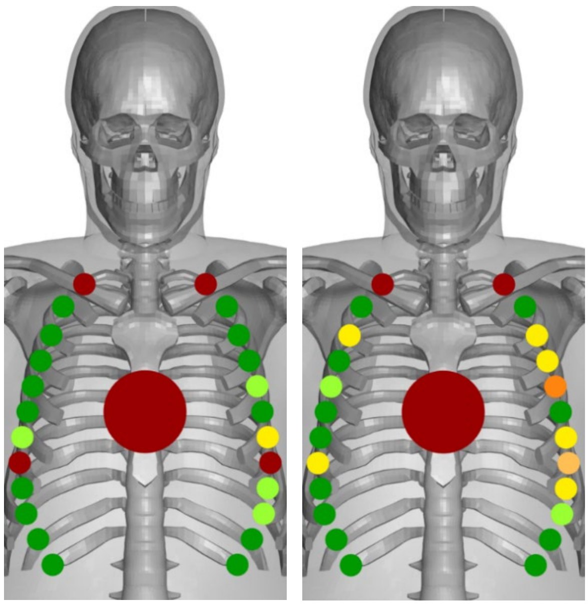

Fig. 10. Study Injury Pattern Difference, outer dots represent predicted rib injury risk, inner dot represents combined probability risk. Green=0-10% predicted injury, Red=50-100% predicted injury. Left: HANS FHR, Right: Hybrid FHR

The seat belt configuration parameter has a similar effect of changing the torso loading pattern, as the 9pt belt, due to reduced engagement of the FHR with the torso, being a wider belt, and having a belt layer under the FHR, significantly reduces the peak thoracic loads as well as spreads out those loads over a larger thoracic area. These effects can be seen in Fig. 11 from a similar overall kinematic response with a raised FHR for the HBM using a 9pt belt (Green), lowering the forces of FHR-HBM engagement. The injury patterns in Fig. 12 reflects these differences, as the 9pt belt case, on the right, has experienced an overall reduced magnitude of strain, as well as a change in injury pattern due to the lack of predicted rib 1 injury.

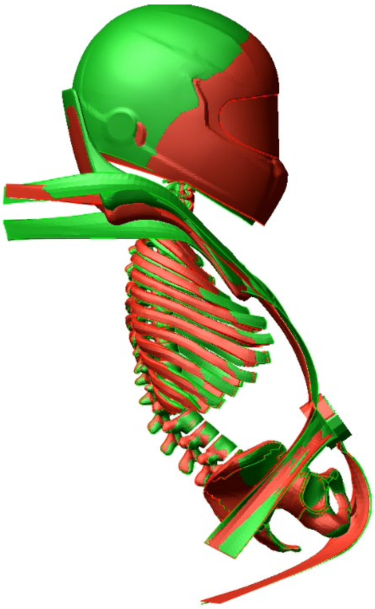

Fig. 11. Study 4 Kinematic Response Difference, Maximum Excursion. Green: 9pt Belt, Red: 7pt Belt.

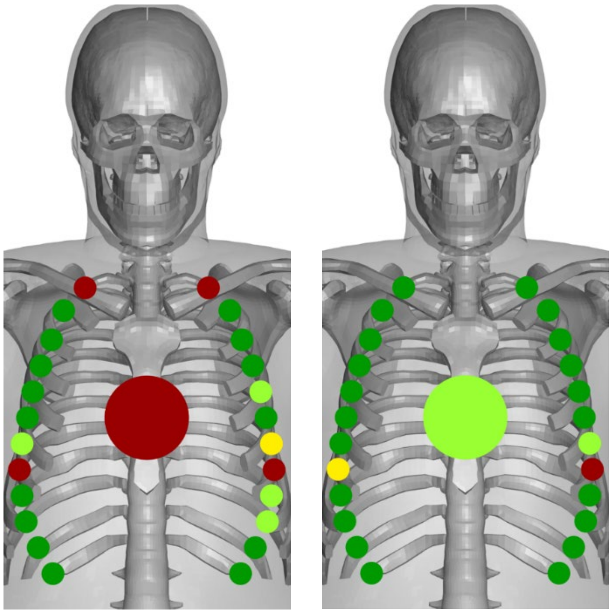

Fig. 12. Study Injury Pattern Difference, outer dots represent predicted rib injury risk, inner dot represents combined probability risk. Green=0-10% predicted injury, Red=50-100% predicted injury. Left: 7pt Belt, Right: 9pt Belt.

Lumbar Injury Prediction

For lumbar injury prediction in sub-study 1, the response to seat foam stiffness is the same as in Fig. 4, where a stiffer seat foam is more protective due to decreased HBM excursion into the seat, which promotes favorable lumbar spine orientation. The main difference for lumbar injury as compared to thoracic injury is the increased effect of HBM mass on predicted injury. For both injury metrics increased HBM mass increases the predicted risk, the effect is magnified for lumbar risk as the increased torso mass greatly increases compression forces and moments in the lumbar region.

The second sub-study regression found that belt tension and material had significant effects on lumbar injury risk, and that increasing belt tension and a softer belt increased predicted injury. As seen in Fig. 13, the overall excursion changes from varied belt tension but the lumbar orientations remain very similar. This effect is negligible due to the low predicted injury range, as well as the predicted injury being on the low end of lumbar fracture risk (25.0-33.5%)

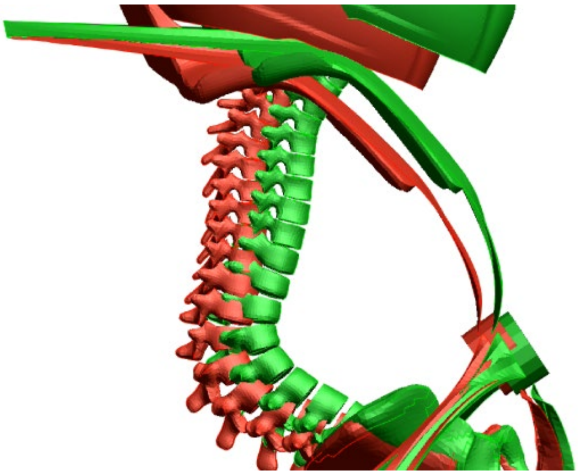

Fig. 13. Study 2 Kinematic Response Difference, Maximum Excursion. Green: -100N, Red: 150N

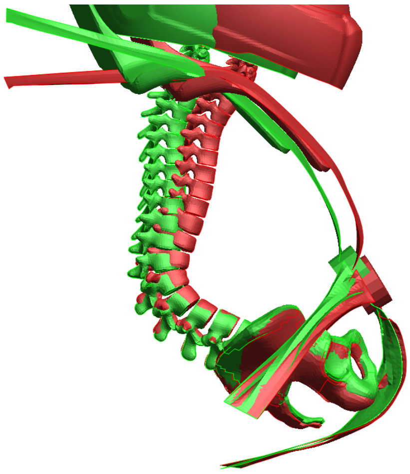

Fig. 14. Study 3 Kinematic Response Difference, Maximum Excursion. Green: 0-degree anchor, Red: 30-degree anchor.

The regressions from sub-studies 3 and 4 predicted more significant effects from parameter variation, with predicted lumbar injury ranges of 30% and 12% respectively. Study 3 predicted similar parameter effects on lumbar injury as for thoracic injury; that more horizontal shoulder belts and more rearward anchored anti-submarine belts are more protective. The mechanism for a more protective rearward anti-submarine belt is the same; additional wrap around the HBM and longer belts contribute additional elongation, reducing the peak loads experienced by the HBM. The shoulder belt effect is different in that a zero degree (horizontal) shoulder belt allows for less upper torso excursion, reducing curvature in the lumbar spine, as can be seen in Fig. 4, and consequently lowering the peak lumbar forces and moments.

Study 4, varying FHR related parameters, predicted only FHR type as a significant parameter affecting lumbar injury. The Hybrid FHR reduces the predicted lumbar injury risk, the opposite effect as for thoracic injury. As seen in Fig. 9, the greatly increased head excursion due to use of the Hybrid FHR positively affects lumbar curvature, reducing the peak loads experienced.

Much of the HBM response was dominated by lumbar spine flexion, especially for thoracolumbar injury prediction. Excessive lumbar spine flexion leads to a loss of tension in the restraint system, increased forward excursion, and abdominal compression. This effect may be a consequence of the formulation of the lumbar spine for the THUMS AM50 v7. The lumbar spine ligaments were validated using data from Chastain *et al*., 2023 with a maximum applied load of 20Nm [21-22]. Burns *et al*., 2024, characterised the lumbar response and found a secondary stiffening region in the flexion moment-angle response past 30Nm of loading [23]. In a comparison of PMHS and HBMs for a reclined occupant condition, Gepner *et al*., 2022 [24] found a significant difference in response of the lumbar spine of HBMs as compared to PMHS. These studies suggest that the lumbar flexion experienced in this condition may be unrepresentative of a PMHS response.

The THUMS specific IRF is one proposed solution to this issue, as it attempts to match force and moment values of fracture to the same flexion angle between PMHS and HBM. This change accounts for the imperfect THUMS biofidelity, though also leads to a lower moment required to predict failure due to THUMS increased tendency for lumbar flexion. Neither usage of the PMHS tuned IRF or THUMS flexion matched IRF are perfect solutions, improvements to the lumbar biofidelity of the THUMS model need to be made for accurate application of IRFs to lumbar fracture.

IV. CONCLUSION

This study replicates a NASCAR racing environment under a complete, parameterized-restraint system, establishing relationships between restraint variation and predicted thoracolumbar injury. HBM based IRFs were used to predict injury in each simulation and develop regressions predicting the effects of parameter variations on injury. An average risk of 55% and 13% were predicted for three plus ribs fractured and lumbar 1 fracture risk functions respectively. Though these injuries have occurred in motorsports, crashes of this severity occur somewhat regularly, and actual injuries of this type are reported infrequently. A study investigating NASCAR injuries over eight seasons documented only two instances of AIS 1+ thoracic injury, though many more crashes occurred at or above the severity of the pulse used for this study [6]. Similar parameter effects on restraint effectiveness were predicted for studies 1 and 3, that stiffer seat foams and horizontal shoulder belt/ rearward anti-submarine belt anchors are more protective. There were differences in the regressions for studies 2 and 4. Thoracic injuries were predicted to be reduced by a polyester belt and higher belt tension, while lumbar injuries were predicted to be slightly increased by higher belt tension, though due to low variation in predicted lumbar injury, low R squared, and dubious lumbar biofidelity, the veracity of this effect is questionable. The predicted effects of FHR variation also differed, with the HANS FHR and 9pt belt being more protective for thoracic injury, and the Hybrid FHR being more protective for lumbar injury. These simulations present an initial exploratory analysis on restraint effectiveness and should not be taken as strict design recommendations. This study established a baseline response for the THUMS AM50 v7 in a NASCAR motorsports environment and examined the sensitivity of thoracic and lumbar injury to 11 different restraint parameters.

V. ACKNOWLEDGEMENTS

This work was supported the by National Association for Stock Car Auto Racing (U.S.A).

VI. REFERENCES

[1] Forman, J. L., McMurry, T. L. (2018) Nonlinear models of injury risk and implications in intervention targeting for thoracic injury mitigation. *Traffic Injury Prevention*, **19**(sup2): pp.S103–S108.

[2] Forman, J., Poplin, G. S., *et al.* (2019) Automobile injury trends in the contemporary fleet: Belted occupants in frontal collisions. *Traffic Injury Prevention*, **20**(6): pp.607–612.

[3] Pipkorn, B., Iraeus, J., *et al.* (2020) Occupant injuries in light passenger vehicles—A NASS study to enable priorities for development of injury prediction capabilities of human body models. *Accident Analysis & Prevention*, **138**: p.105443.

[4] Pintar, F. A., Yoganandan, N., *et al.* (2012) Thoracolumbar spine fractures in frontal impact crashes. *Annals of Advances in Automotive Medicine*, **56**: pp.277–283.

[5] Shaikh, J., Thathia, H., & Lubbe, N. (2020, April). *Lumbar Spine Injuries in Motor Vehicle Crashes*. IRCOBI Asia 2020, Beijing, China.

[6] Patalak, J. P., Harper, M. G., *et al.* (2020) Estimated crash injury risk and crash characteristics for motorsport drivers. *Accident Analysis & Prevention*, **136**: p.105397.

[7] Patalak, J. (2013) Examination of a properly restrained motorsport occupant. *SAE International Journal of Transportation Safety*, **1**(2): pp.261–277.

[8] Forman, J., Kulkarni, S., *et al.* (2022) A method for thoracic injury risk function development for human body models. Proceedings of the International Research Council on Biomechanics of Injury Conference, 2022, Porto, Portugal.

[9] Tushak, S. K., Gepner, B. D., *et al.* (2023) Human lumbar spine injury risk in dynamic combined compression and flexion loading. *Annals of Biomedical Engineering*, **51**(6): pp.1216–1225.

[10] Morgan, N. R., Lovenduski, C. A., *et al.* (2026) Instrumentation and analysis of THUMS simulations for whole body injury prediction. Proceedings of the International Technical Conference on the Enhanced Safety of Vehicles, 2026, Toronto, Canada.

[11] Håland, Y. (2006) The evolution of the three point seat belt from yesterday to tomorrow. Proceedings of the International Research Council on Biomechanics of Injury Conference, 2006, Madrid, Spain.

[12] Melvin, J. W., Little, W. C., *et al.* (1994) Racing car restraint system frontal crash performance testing. Proceedings of the SAE International Congress and Exposition, 1994, Detroit, Michigan, US.

[13] Grzebieta, R., Rechnitzer, G., *et al.* (2017) Development of proposed dynamic crash tests and performance criteria for the Australian concession go-karts standard. Proceedings of the International Technical Conference on the Enhanced Safety of Vehicles, 2017, Detroit, Michigan, US.

[14] Mertz, H. J. (2002) Anthropomorphic test devices. In Nahum, A. M., Melvin, J. W. (eds.) *Accidental Injury: Biomechanics and Prevention*, pp.72–88. Springer, New York.

[15] Rawska, K., Tushak, S. K., *et al.* (2026) Biofidelity evaluation and injury risk function development for THUMS AM50 v7 under compression–flexion lumbar spine loads. Proceedings of the International Research Council on Biomechanics of Injury Conference, 2026, Munich, Germany.

[16] Fox, J. (2016) *Applied Regression Analysis and Generalized Linear Models*, 3rd ed. SAGE Publications, Thousand Oaks.

[17] Johnson, R. A., Wichern, D. W. (2007) *Applied Multivariate Statistical Analysis*, 6th ed. Pearson Prentice Hall, Upper Saddle River.

[18] SFI Foundation Inc. (2013) SFI specification 45.2: Quality assurance specification. SFI Foundation Inc., Indianapolis.

[19] Gray, A. N., Harper, M. G., *et al.* (2025) Development and validation of a rear head surround foam performance specification for stock car racing. *SAE International Journal of Vehicle Safety*.

[20] Weerappuli, P., Prasad, P., Barbat, S. (2005) Effectiveness of the head and neck support (HANS) device in frontal impacts of CART cars: A CAE analysis. *International Journal of Vehicle Safety*, **1**(1–3): pp. pp 129–144.

[21] Chastain, K., Gepner, B., *et al.* (2023) Effect of axial compression on stiffness and deformation of human lumbar spine in flexion–extension. *Traffic Injury Prevention*, **24**(sup1): pp.S55–S61.

[22] Matsuda, T., Kobayashi, N., *et al.* (2023) Development of a human body model (THUMS version 7) to simulate kinematics and injuries of reclined occupants in frontal collisions. Proceedings of the International Technical Conference on the Enhanced Safety of Vehicles, 2023, Yokohama, Japan.

[23] Burns, M. R., Caldwell, A. J., Sochor, S. H., Shin, J., Hanggi, C. J., Gepner, B., & Kerrigan, J. R. (2024, September 11). *Lumbar Spine Mechanical Response to Combined Flexion and Compression in Post-Mortem Human Subjects*. IRCOBI 2024, Stockholm, Sweden.

[24] Gepner, B. D., Perez-Rapela, D., *et al.* (2022) Evaluation of GHBMC, THUMS and SAFER human body models in frontal impacts in reclined postures. Proceedings of the International Research Council on Biomechanics of Injury Conference, 2022, Porto, Portugal.

[25] Patalak, J. P., & Stitzel, J. D. (2018). Evaluation of the effectiveness of toe board energy-absorbing material for foot, ankle, and lower leg injury reduction. *Traffic Injury Prevention*, *19*(2), 195–200.

[26] Patalak, J., Davis, M., Gaewsky, J., Stitzel, J., & Harper, M. (2018). *Influence of Driver Position and Seat Design on Thoracolumbar Loading During Frontal Impacts*. 2018-01–0544.

VII. APPENDIX

Appendix A: Belt Anchor Location Details

Fig. A1. Shoulder belt anchor locations

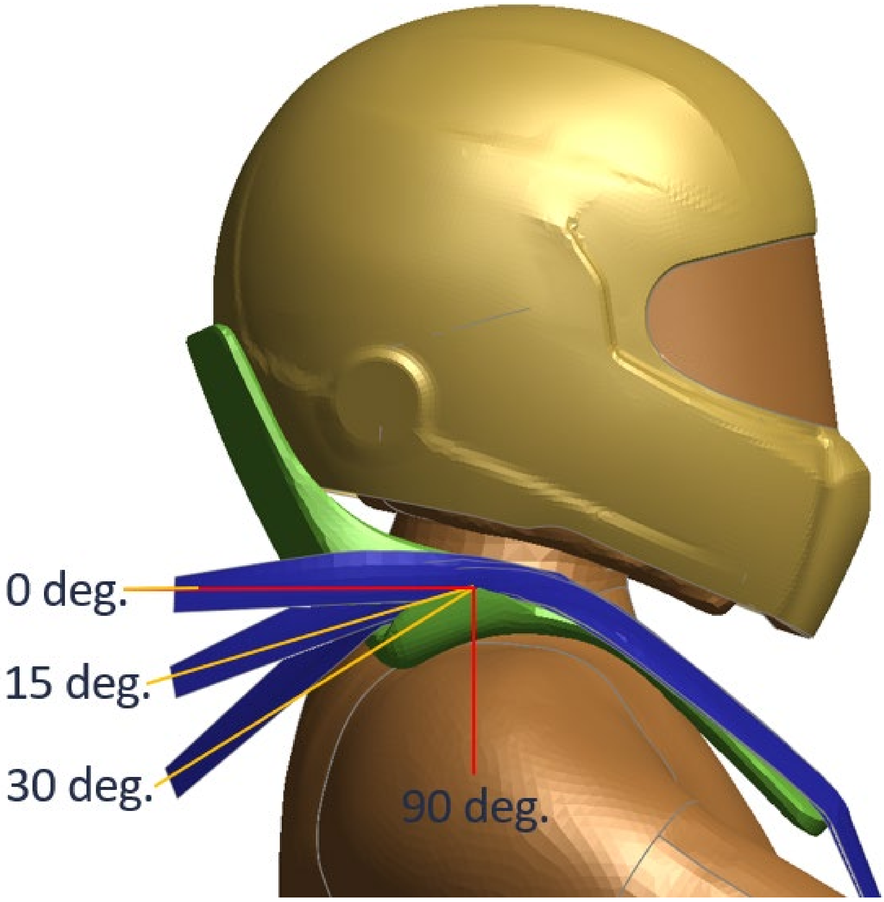

Fig. A2. Lap belt anchor locations

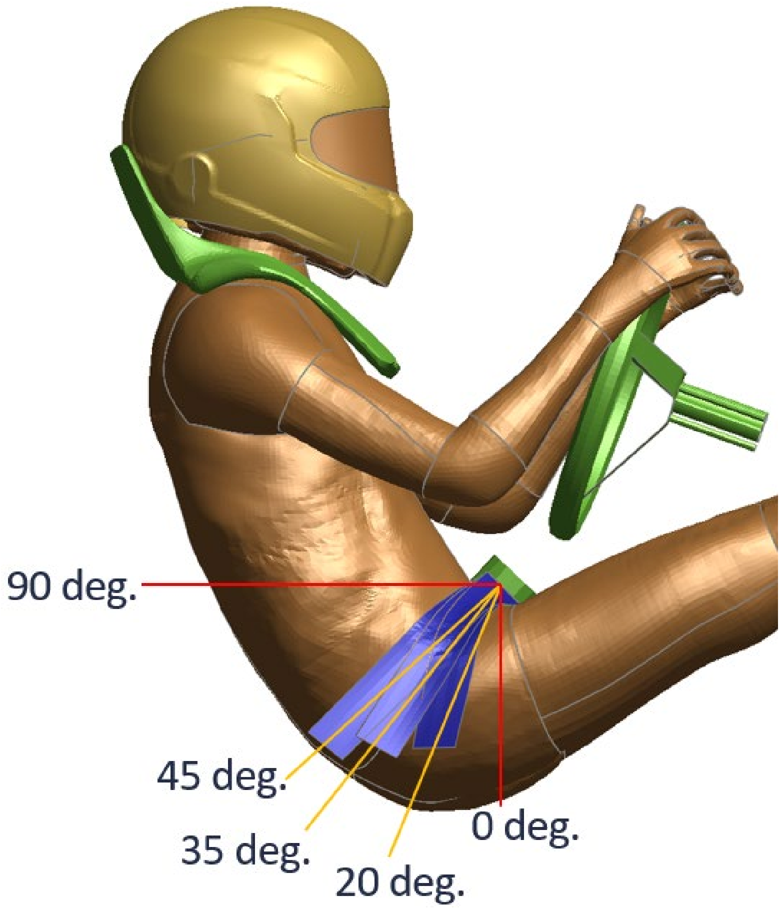

Fig. A3. Anti-submarine belt anchor locations

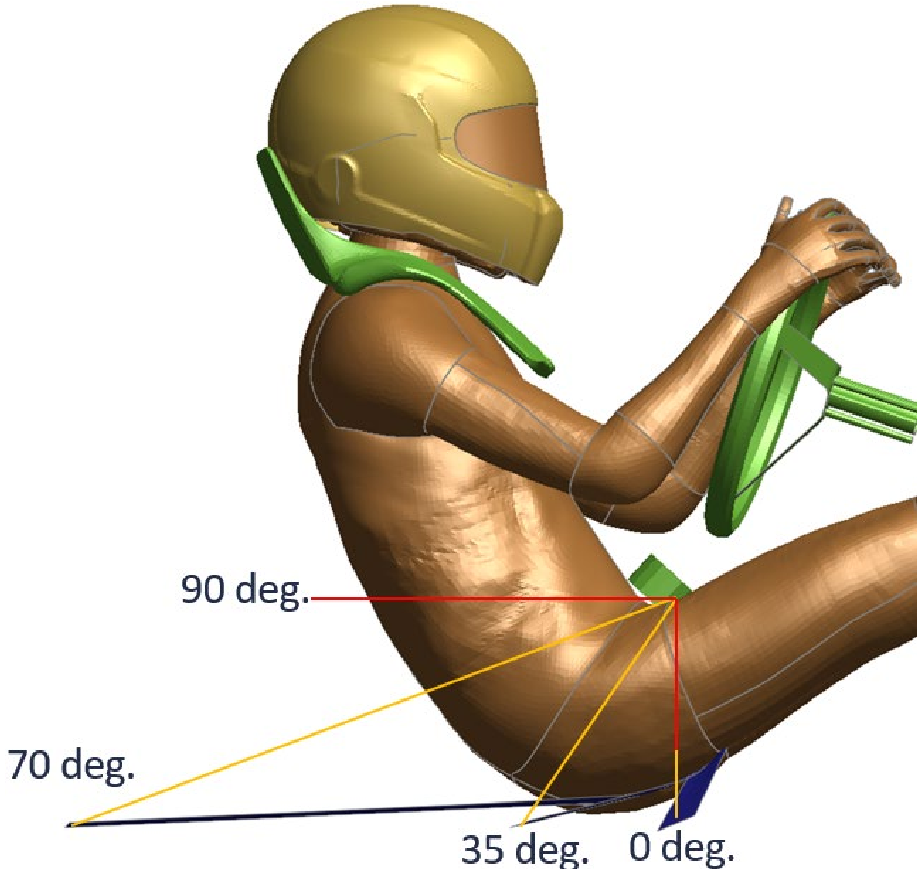

Fig. A4. 9pt shoulder belt anchor locations

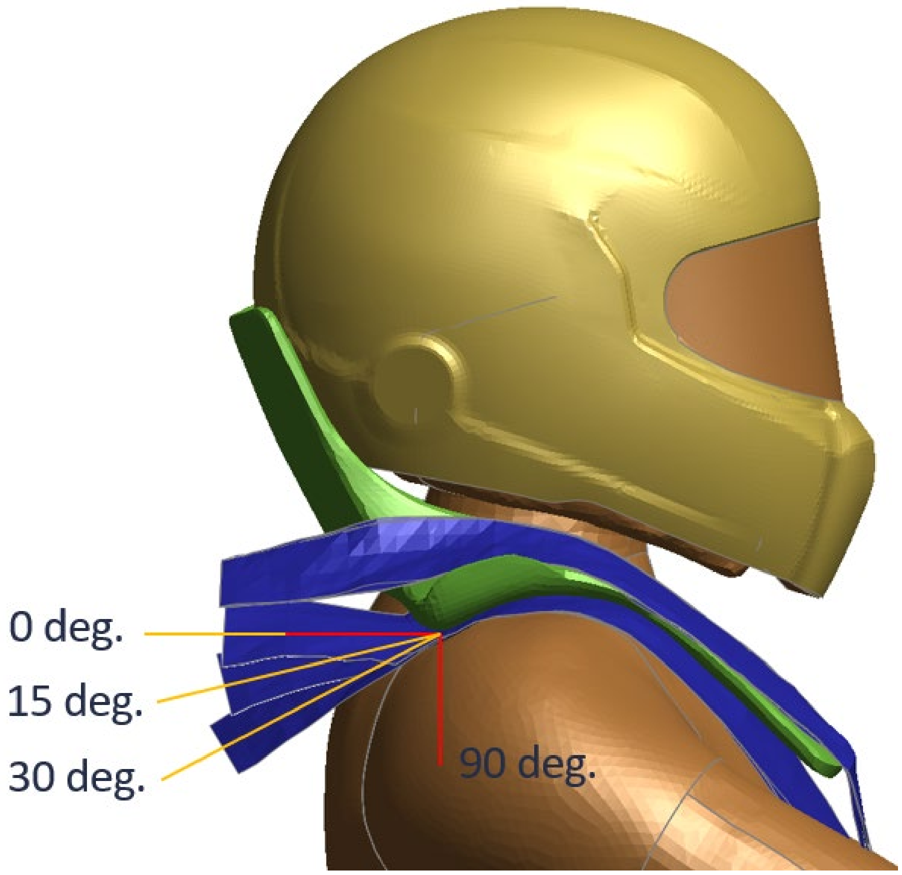

Fig. A5. 9pt shoulder belt

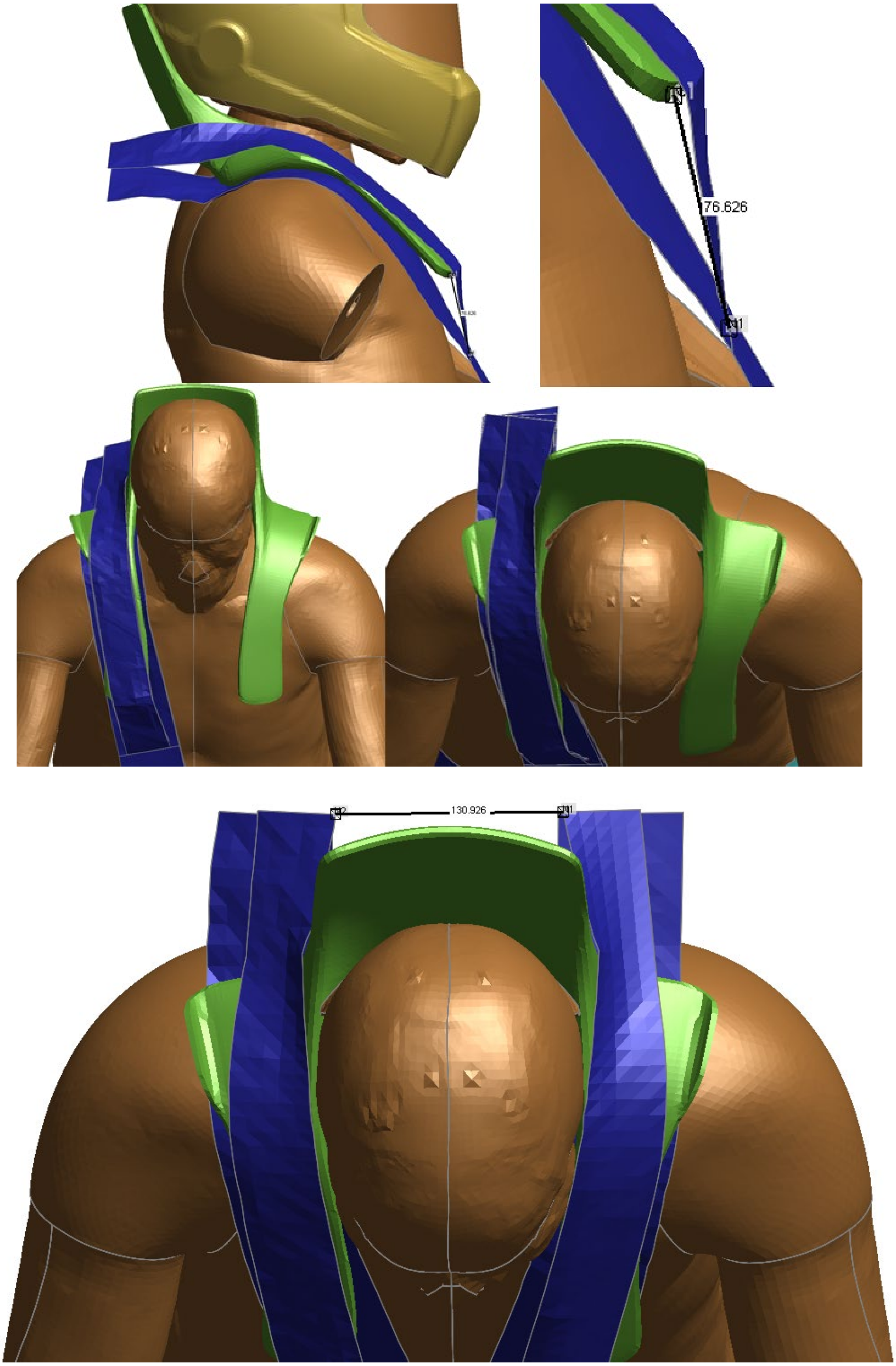

Fig. A6. Hybrid FHR

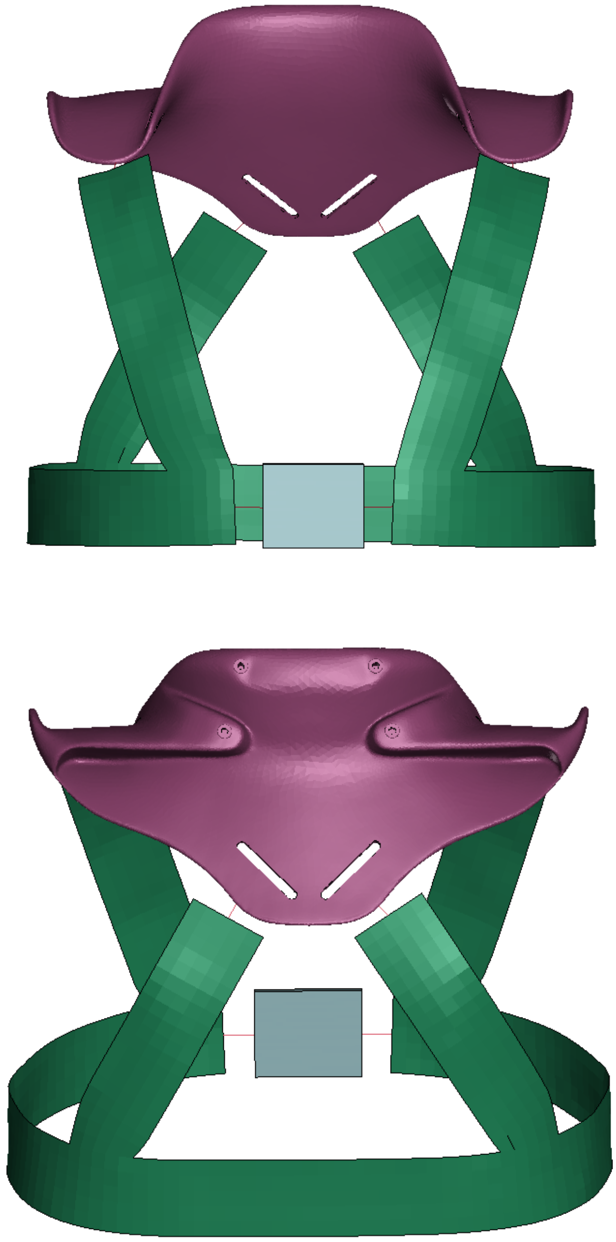

Appendix B: Seat Belt Material Models

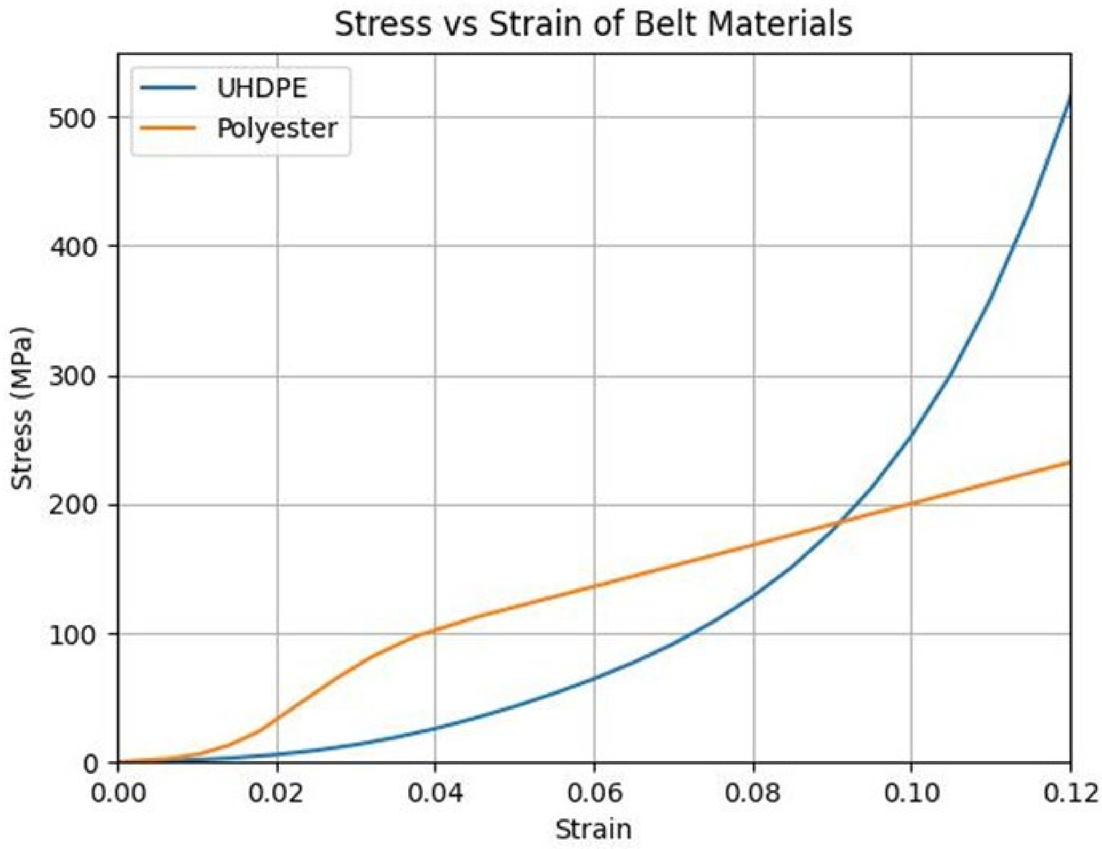

Appendix C: Pulse

Fig. C1. Simulation Pulse Severity Compared to NASCAR Crashes From 2011-2018 [6]

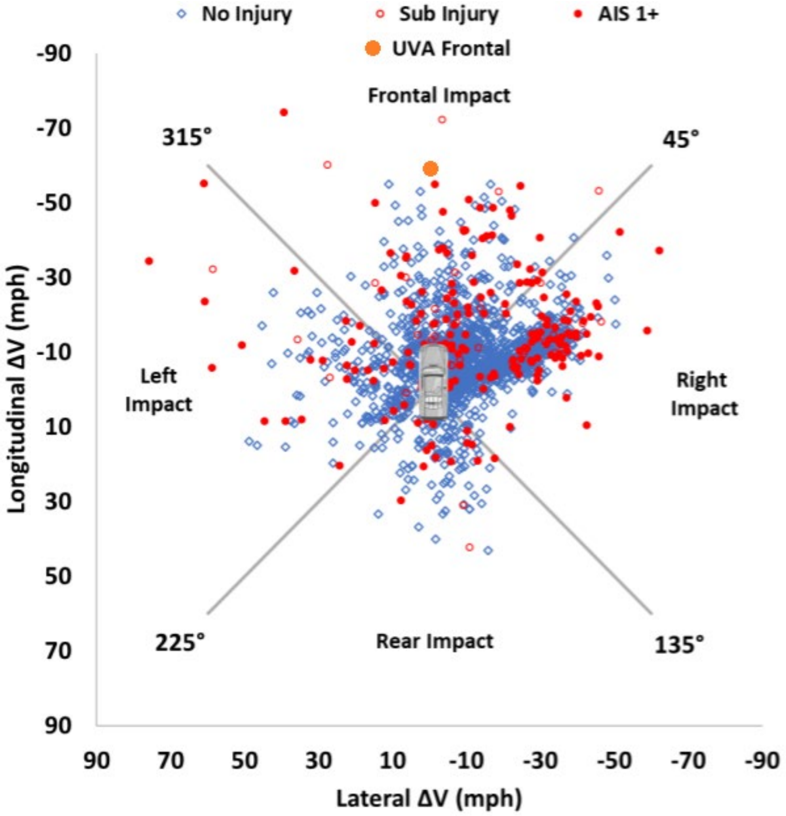

Fig. C2. Simulation Pulse Applied Acceleration (G's)

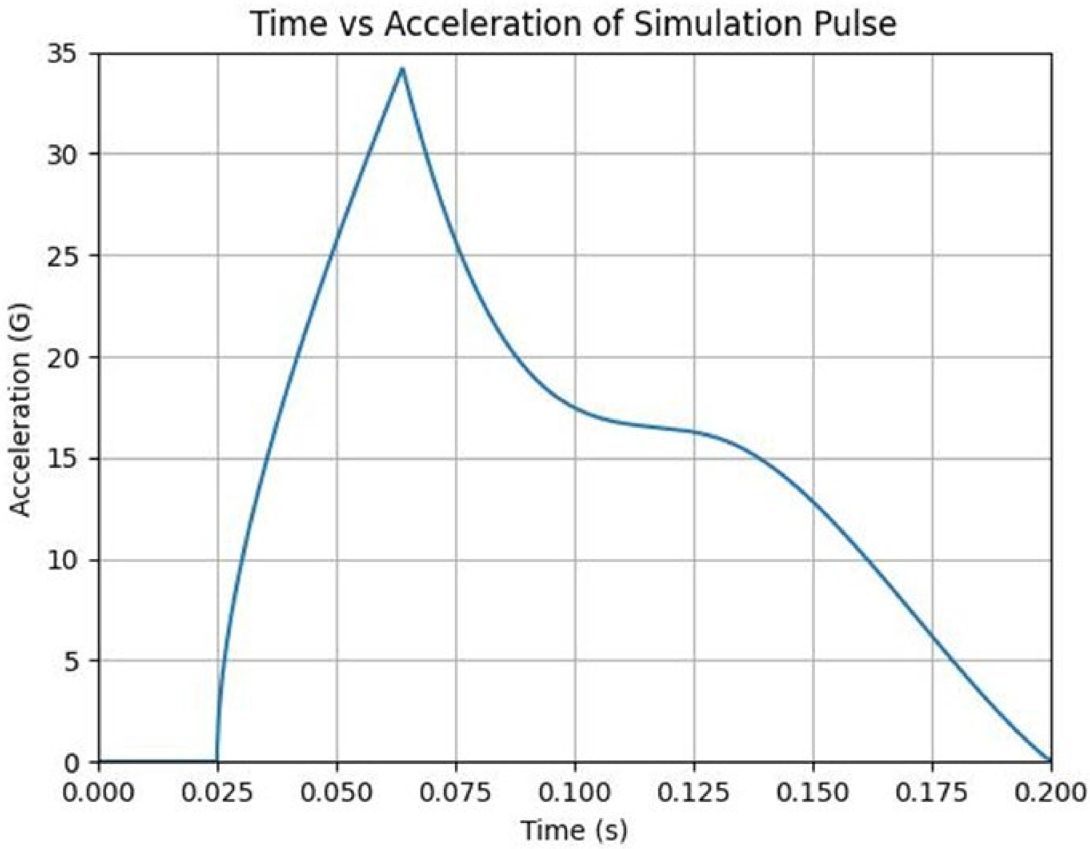

Appendix D: Lumbar IRF

Fig D1. Injury probability for the THUMS as a function of Lfx, for an age of 45 years. Mean with 95% confidence intervals. Individual data points at y=0 for non-middle vertebra injury (right-censored) or y=1 for middle vertebra injury (uncensored or left-censored).

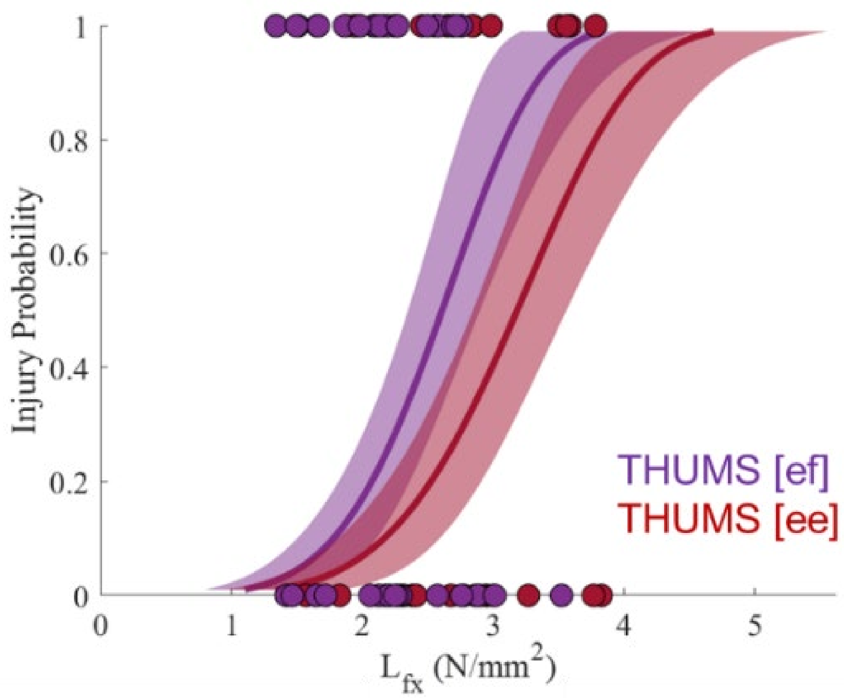

Fig D.2 Lumbar Vertebrae Cross Sectional Areas and Lever Arms for the THUMS v7.1 AM50, Used in Lfx Calculations

THUMS AM50 Lumbar Vertebrae Cross Sectional Area

Vertebrae	Cross Sectional Area (mm^2)	Lever Arm Distance (mm)
L1	1154.85	18.11
L2	1301.49	16.29
L3	1364.20	15.14
L4	1379.74	17.65
L5	1378.46	18.04

Appendix E: Rib Strain Comparisons

Fig E.1: Strains from Fig. 4. Left: Stiffer Seat Foam (SFI 45.2), Right: Softer Seat Foam (NASCAR Option 2).

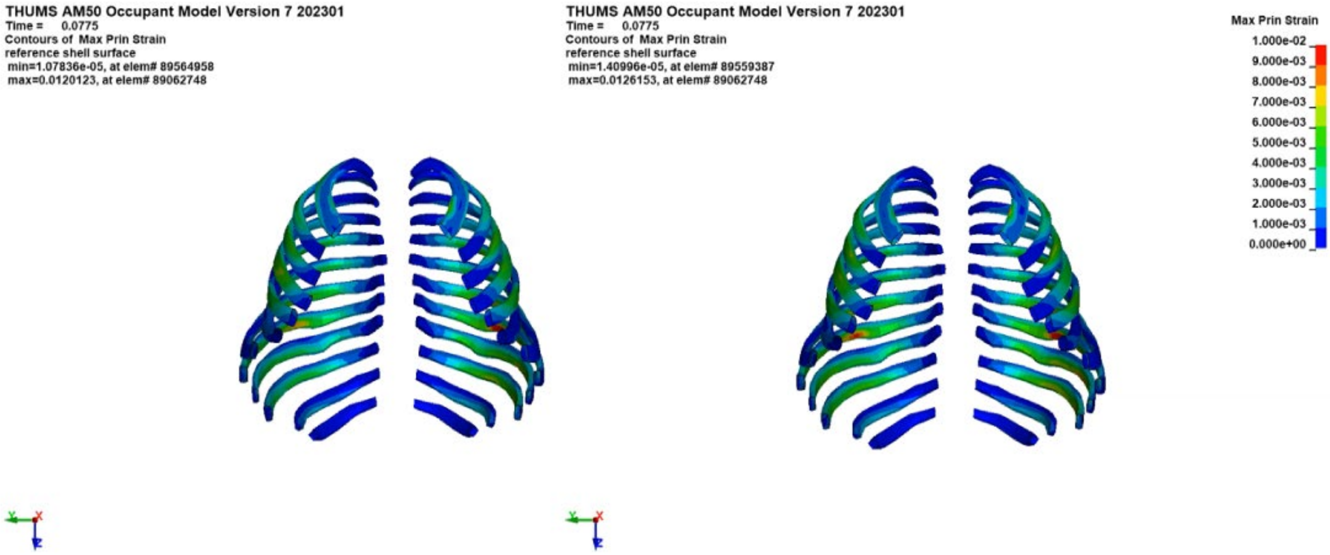

Fig E.2: Strains from Fig. 5. Left: -100N Belt Tension, Right: 150N Belt Tension.

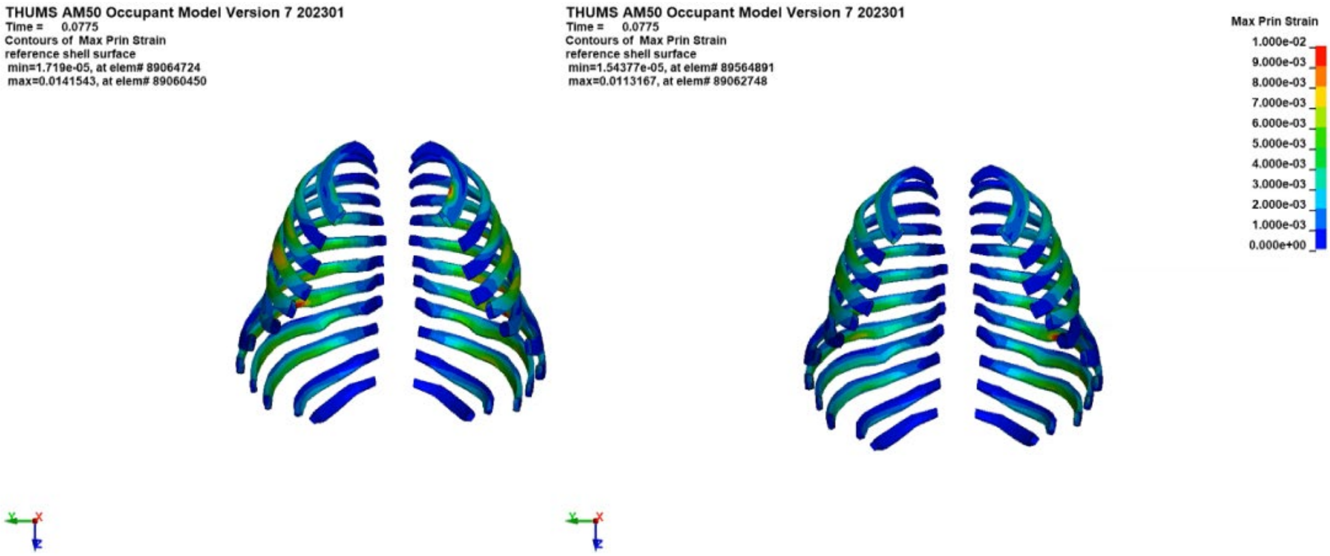

Fig E.3: Strains from Fig. 6. Left: polyester belt, Right: UHDPE belt

Fig E.4: Strains from Fig. 7. Left: 0-degree shoulder belt anchor, Right: 30-degree shoulder belt anchor.

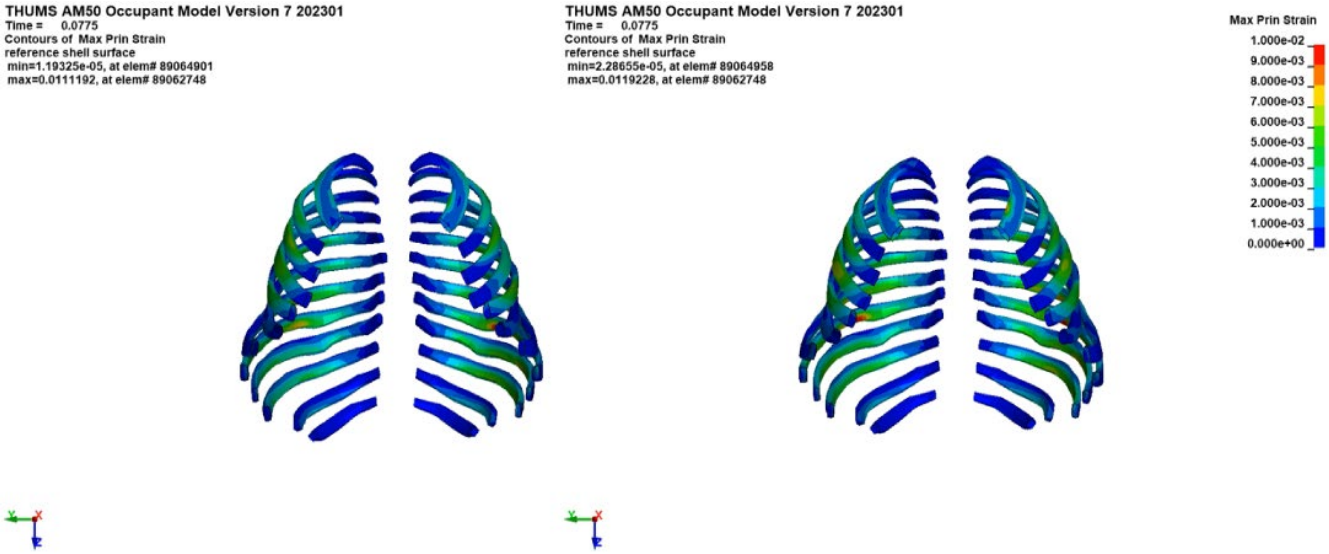

Fig E.5: Strains from Fig. 8. Left: 0-degree anti-submarine belt anchor, Right: 70-degree anti-submarine belt anchor.

Fig E.6: Strains from Fig. 9. Left: HANS FHR, Right: Hybrid FHR.

Fig E.7 Strains from Fig. 11. Left: 7pt Belt, Right: 9pt Belt.